FR-PHENO-2010-016

Electroweak and Bottom Quark Contributions to Higgs Boson plus Jet Production

Oliver Brein

Physikalisches Institut, Albert-Ludwigs-Universität Freiburg
Hermann-Herder-Str. 3, D-79104 Freiburg im Breisgau, Germany

Oliver.Brein@physik.uni-freiburg.de

Abstract

This paper presents predictions for jet pseudorapidity (η) and transverse momentum (p_T) distributions for the production of the Standard Model Higgs boson in association with a high-p_T hadronic jet. We discuss the contributions of electroweak loops and of bottom-quark parton processes to the cross section. The latter arise in the five-flavour scheme. Predictions for the Tevatron and the Large Hadron Collider with 10 TeV collision energy are presented. For Higgs boson masses of 120 GeV, 160 GeV and 200 GeV, we find the maximal effects of the electroweak contributions to the Higgs plus jet p_T and η distribution to be -14% and -5.3%, respectively, for the Tevatron, and -3% and -2%, respectively, for the LHC. For the maximal contribution of bottom-quark parton processes to the p_T and η distribution, we find $+3\%$ and $+2.5\%$, respectively, for the Tevatron, and $+3.5\%$ and $+3\%$, respectively, for the LHC. A separate study of the Higgs + b-jet cross section demonstrates that a calculational approach which respects the hierarchies of Yukawa couplings yields a leading order cross section prediction which is more accurate in the high-p_T regime than conventional approaches.

1 Introduction

Since the discovery of the massive electroweak gauge bosons Z and $W^{\pm}$ [1], we are sure to observe electroweak symmetry breaking in nature. However, the underlying dynamics of this symmetry breaking has not yet been established experimentally. Spontaneous symmetry breaking via the Higgs mechanism [2] is an appealing theoretical suggestion for such a dynamics. Depending on the specific model considered, the Higgs mechanism implies the existence of one or more scalar particles (Higgs bosons). Therefore, the search for Higgs bosons is an important task in the quest to unravel the nature of electroweak symmetry breaking at high energy collision experiments.

Besides inclusive single Higgs production, Higgs boson production in association with a high-p_T hadronic jet provides a useful channel for Higgs searches at hadron colliders, which allows for refined cuts increasing the signal-to-background ratio. Specifically, for the Standard Model (SM) Higgs plus jet process [3, 4], early simulations considering the decay channels $H \to \gamma\gamma$ [5, 6] and $H \to \tau^+\tau^-$ [7] have demonstrated promising signal-to-background ratios. While the promising findings of the parton-level study [5] were confirmed by a simulation using the fast (and less detailed) simulation for the ATLAS detector response [6], an up-to-date simulation of the detailed ATLAS detector performance appeared in [8]. From the CMS collaboration, only a simulation of the inclusive $H \to \gamma\gamma$ channel is currently available [9].

Considerable progress has been made in improving the SM cross section predictions: The fully differential distribution for Higgs production is available at next-to-next-to-leading order (NNLO) QCD accuracy in the large top-mass limit [10], improved by the resummation of logarithmically enhanced terms for low p_T [11]. Dedicated calculations of higher-order corrections to differential cross sections for Higgs boson production associated with a high-p_T jet have been performed: the next-to-leading order (NLO) QCD corrections in the large top-mass limit [12] and the corresponding resummation of large threshold logarithms [13]. Furthermore, the soft-plus-virtual gluon approximation to the NLO QCD prediction of the Higgs p_T distribution [14] goes beyond the large top-mass limit. For the b-quark process $bg \to Hb$, the NLO QCD corrections are also known [15, 16], and very recently a calculation of the weak corrections to this process appeared [17].

The remaining scale uncertainty of the NLO QCD result for the Higgs plus high-p_T jet production cross section via the light quark parton processes is at the level of 10% [12, 13]. The achievement of this level of accuracy in the QCD corrections, albeit in the large top-mass limit, motivates to study other leading order contributions which could potentially affect the Higgs plus jet cross section prediction at the 10% level. Specifically, there are to consider: loop-induced electroweak contributions to the processes $qg \to Hq$ and $q\bar{q} \to Hg$ for the light quark flavours (u, d, s, c) and the contributions from the processes $bg \to Hb$ and $b\bar{b} \to Hg$. All these contributions may change the differential distributions of the process, which are therefore of particular interest. Parts of these contributions to the Higgs plus jet cross section have been considered elsewhere. Electroweak and non-zero quark-mass effects on the Higgs p_T distribution using 5-flavour parton distribution functions (PDFs) neglecting the contributions from b-quark parton processes have been studied for the LHC

and the Tevatron in [18]. Leading order QCD and electroweak contributions to the qg and $q\bar{q}$ processes, including electroweak contributions to the b-quark processes enhanced by the top-Higgs Yukawa coupling, have been studied for the LHC in [19]. However, the impact of those contributions on the total Higgs plus jet cross section, which involves also the dominant gluon fusion channel, has not been studied in [19]. To our knowledge, a combination of the contributions of the light quark flavours (u, d, s, c) and the bottom quarks in order to get a cross section prediction for Higgs plus (any) jet in a 5-flavour scheme has so far only been done for the leading-order QCD predictions [20, 21].

In the present paper, we study the combined effect of contributions of leading order (LO) electroweak loop graphs and bottom-quark parton processes on the jet pseudorapidity (η) and transverse momentum (p_T) distribution of Higgs + high-p_T jet production.

In order to obtain the best LO prediction, we employ a somewhat different scheme than usual, which particularly affects the bottom-quark processes. Instead of discarding higher order contributions in the cross section predictions according to mere power counting of QCD and electroweak couplings (g_S, e), regardless of the appearing type of Yukawa coupling (y_b, y_t), we argue that keeping the LO contributions to each monomial in y_b and y_t and discarding the higher order contributions to each of them separately, gives a more accurate approximation to the full result. This approach is particularly well-suited for the bottom-quark processes, because in this case tree-level graphs $\propto g_S y_b$ and one-loop graphs $\propto g_S^3 y_t$ contribute and just discarding the loop-contributions because of the higher power of g_S does not do justice to the hierarchy of Yukawa couplings $y_t \gg y_b$ in the Standard Model.

As the Higgs plus b-jet final state is also of separate interest, in particular in models beyond the SM, where the top and bottom Yukawa couplings can be dramatically different, we discuss this process also separately in appropriate places below.

Section 2 briefly reviews the contributing parton processes and Section 3 gives details on our calculational approach. In Section 4 we present numerical results for the distributions at the LHC and the Tevatron and Section 5 contains our conclusions.

2 Partonic Processes

At the partonic level, production of a Higgs boson H together with a jet at hadron colliders is mediated by three classes of processes (see Fig. 1):

gluon fusion	$g + g \to g + H\,,$
quark–gluon scattering	$q(\bar{q}) + g \to q(\bar{q}) + H\,,$
quark–anti-quark annihilation	$q + \bar{q} \to g + H\,.$

For the gluon fusion channel, the leading order contribution to the cross section prediction is of order $\alpha_S^3\alpha$ in the strong and electromagnetic coupling constants α_S and α. The corresponding Feynman graphs have one-loop topologies and are displayed in Fig. 1(a), where the shaded blobs represent triangle- and box-type loops of virtual quarks. The loop contributions can be further subdivided according to their scaling with the quark Yukawa

couplings $y_q = \frac{e}{2s_W}\frac{m_q}{m_W}$, or equivalently $\alpha_q := y_q^2/4\pi$, appearing in the mathematical expression for the amplitude. Naturally, the dominant cross section contribution ($\propto \alpha_S^3\alpha_t$) comes from top-quark loops in the SM. However, as has been demonstrated e.g. in [18], including bottom-quark loops ($\propto \alpha_S^3\alpha_b$) changes the gluon fusion cross section by several percent. There is no electroweak contribution to gluon fusion at one-loop order.

For quark–gluon scattering and quark–anti-quark annihilation of light quarks (u, d, s, c), the leading order QCD cross section prediction is also loop-induced and of order $\alpha_S^3\alpha_q$, where only the α_t and α_b terms are relevant. The prediction is calculated from the graph topologies displayed in Figs. 1(b) and 1(c) with triangle-type loops of heavy quarks as subgraphs. The Feynman graphs for the process $\bar{q}g \to H\bar{q}$ is obtained by crossing the appropriate quark lines in Fig. 1(b). In contrast to gluon fusion, these two reactions are also mediated by electroweak one-loop graphs $\propto g_S e^3$. Fig. 2 exemplarily shows the full set of Feynman graphs for the scattering of an up-type quark with a gluon. The corresponding Feynman graphs for the processes $\bar{u}g \to H\bar{u}$ and $u\bar{u} \to Hg$ can be obtained by crossing the appropriate external lines in Fig. 2.

In the five-flavour scheme, also b-quark initiated processes for quark–gluon scattering and quark–anti-quark annihilation contribute to the Higgs plus jet cross section. For bottom–gluon scattering and $b\bar{b}$ annihilation, the QCD leading order cross section prediction is $\propto \alpha_S\alpha_b$ and comes from tree-level Feynman graphs shown in Fig. 1(d). Because of the hierarchy of Yukawa couplings, loop-induced QCD and electroweak contributions to the b-quark parton processes, which contain a factor α_t, can be as important as the tree level contribution in the SM [19]. The QCD contributions to bg scattering and $b\bar{b}$ annihilation are shown in Fig. 1(b) and Fig. 1(c), respectively, where the external quarks are b quarks and the shaded blob represents triangle-type loops of virtual top-quarks.[1] The Feynman graphs are $\propto g_S^3 y_t$. The electroweak contributions to bg scattering which do not vanish for $m_b = 0$ are shown in Fig. 3. The contributions to the $\bar{b}g \to H\bar{b}$ and $b\bar{b} \to Hg$ amplitudes can be obtained by crossing the appropriate external lines in Fig. 3. The first two rows of Feynman graphs in Fig. 3 are proportional to the top-quark Yukawa coupling y_t. We do not consider graphs $\propto y_b$ here, as they only form a part of the subleading electroweak contribution $\propto \alpha_S\alpha\alpha_b$ to the cross section prediction and cannot be considered separately.

The b-quark initiated processes are usually not considered a relevant contribution to the Higgs plus jet final state in the Standard Model (SM), but may even become dominant in models beyond the SM with a strongly enhanced bottom-Higgs Yukawa coupling. This is for instance the case in the Minimal Supersymmetric Standard Model (MSSM) for the lightest MSSM Higgs boson for low values of the A-boson mass m_A ($\lesssim 120\,\text{GeV}$) [20, 21, 22, 23]. However, in our calculation, we include the b-quark parton processes in the Higgs plus jet cross section calculation in order to assess the size of their contribution in comparison with taking effects of a non-vanishing bottom-Higgs Yukawa-coupling into account in the

[1] The same contribution with a virtual bottom instead of a top quark is only part of the subleading QCD contribution $\propto \alpha_S^2\alpha_b$ to the cross section prediction and cannot be considered separately. While the interference of this particular graph with the tree-level QCD amplitude in our approach (y_b non-zero and $m_b = 0$ otherwise, to be explained in the next Section) vanishes, there are more one-loop graphs which contribute to QCD correction of that order.

loop-induced light-quark parton processes.

3 Calculational Approach

For perturbative predictions involving Higgs bosons, the Higgs couplings to other particles, which are proportional to their mass, create further hierarchies within loop-contributions in addition to the power series in the QCD and the electromagnetic coupling constant α_S and α. Therefore, it is useful to judge the importance of contributions also according to the hierarchy of Yukawa coupling constants $\alpha_q = y_q^2/4\pi = \frac{1}{4\pi} m_q^2/v^2$ ($v = 246\,\mathrm{GeV}$) which is induced by the hierarchy of quark masses m_q. For the two heaviest quarks, this hierarchy is even more pronounced than the hierarchy between radiative corrections of consecutive perturbative QED orders. In fact, for our choice of mass parameters (see below) we get $\alpha_t = 3.9 \cdot 10^{-2}$ and $\alpha_b = 2.3 \cdot 10^{-6}$ and $\alpha_b/\alpha_t \approx (\alpha(0))^2 < (\alpha_S(m_Z))^4$.

In order to provide an overview of the leading order contributions to the Higgs plus jet production channels subdivided by the hierarchy of Yukawa couplings, we provide symbolic equations for the scattering amplitudes and the squared matrix elements which highlight the dependence on the coupling constants. The scattering amplitudes we consider have the form:

$$\mathcal{M}_{gg} = A_t g_S^3 y_t + A_b g_S^3 y_b \,, \tag{1}$$

$$\mathcal{M}_X(q) = B_X^t(q) g_S^3 y_t + B_X^b(q) g_S^3 y_b + C_X(q) g_S e^3 \,, \tag{2}$$

$$\mathcal{M}_X(b) = D_X(b) g_S y_b + B_X^t(b) g_S^3 y_t + E_X^t(b) g_S e^2 y_t + (C_X(b) + F_X(b))\, g_S e^3 \,, \tag{3}$$

with $X \in \{qg, \bar{q}g, q\bar{q}\}$ and $q = u, d, s, c$. The squared matrix elements, only keeping non-vanishing contributions for $m_b = 0$ while retaining α_b non-zero (explanation follows below), read:

$$|\mathcal{M}_{gg}|^2/(4\pi)^4 = \alpha_t |A_t|^2 \alpha_S^3 + \alpha_b |A_b|^2 \alpha_S^3 + \sqrt{\alpha_t \alpha_b}\, 2\mathrm{Re}[A_t^\star A_b] \alpha_S^3 \,, \tag{4}$$

$$\begin{aligned} |\mathcal{M}_X(q)|^2/(4\pi)^4 = {} & \alpha_t |B_X^t(q)|^2 \alpha_S^3 + \alpha_b |B_X^b(q)|^2 \alpha_S^3 \\ & + \sqrt{\alpha_t \alpha_b} \Big\{ 2\mathrm{Re}\Big[(B_X^t(q))^\star B_X^b(q) \Big] \alpha_S^3 \Big\} \\ & + \sqrt{\alpha_t} \Big\{ 2\mathrm{Re}\Big[(B_X^t(q))^\star C_X(q) \Big] \alpha_S^2 \alpha \sqrt{\alpha} \Big\} \\ & + \sqrt{\alpha_b} \Big\{ 2\mathrm{Re}\Big[(B_X^b(q))^\star C_X(q) \Big] \alpha_S^2 \alpha \sqrt{\alpha} \Big\} \\ & + |C_X(q)|^2 \alpha_S \alpha^3 \,, \end{aligned} \tag{5}$$

$$
\begin{aligned}
|\mathcal{M}_X(b)|^2/(4\pi)^4 = {} & \alpha_t \Big\{ |B_X^t(b)|^2 \alpha_S^3 + 2\mathrm{Re}\Big[(B_X^t(b))^\star {E_X}^t(b) \Big] \alpha_S^2 \alpha + |E_X^t(b)|^2 \alpha_S \alpha^2 \Big\} \\
& + \alpha_b \Big\{ |D_X(b)|^2 \alpha_S \Big\} (4\pi)^{-2} \\
& + \sqrt{\alpha_t} \Big\{ 2\mathrm{Re}\Big[(B_X^t(b))^\star (C_X(b) + F_X(b)) \Big] \alpha_S^2 \alpha \sqrt{\alpha} \\
& \qquad + 2\mathrm{Re}\Big[(E_X^t(b))^\star (C_X(b) + F_X(b)) \Big] \alpha_S \alpha^2 \sqrt{\alpha} \Big\} \\
& + |C_X(b) + F_X(b)|^2 \alpha_S \alpha^3 \,.
\end{aligned}
\tag{6}
$$

For the b-quark processes, the interference between the tree level graphs (see Fig. 1(d)) and one-loop QCD (see Figs. 1(b),(c)) and electroweak graphs (see Fig. 2) vanishes for $m_b = 0$.

In order to provide an accurate prediction of all QCD and electroweak leading order contributions to the Higgs plus jet cross section, respecting the Yukawa hierarchies, we choose the following approach. In the squared amplitude of each process we take into account the full polynomial in $\sqrt{\alpha_t}$ and $\sqrt{\alpha_b}$, i.e. we do not discard terms according to mere QCD power counting. Beyond leading order, this approach would amount to a reordering of the perturbative expansion, where corrections to each of the appearing monomials in $\sqrt{\alpha_q}$ (mainly $q = t, b$) has a separate power series in the QCD and electromagnetic coupling constant. Furthermore, e.g. for processes with external b-quarks, additional positive powers of m_b ($= v y_b$) can appear in squared matrix elements from interference terms. In such cases, a consistent expansion of the massive-quark squared matrix element in m_b, regardless whether it occurs in the coupling constant $\sqrt{\alpha_b}$ or directly, has to be performed.[2]

That this approach is adequate for a study of all relevant leading contributions is confirmed by the comparably large relative size of the squared and interference contributions of the different terms of the amplitude in Eqs. (5) and (6) to the cross section prediction. As an example, Fig. 4 demonstrates this behaviour for bottom-gluon parton scattering for $m_H = 120\,\mathrm{GeV}$ and a cut on the scattering angle $10^\circ < \hat{\theta} < 170^\circ$. While the top-loop squared contribution is quite large throughout the displayed centre-of-mass energy $\sqrt{\hat{s}}$, also the contribution of the squared electroweak loops reach more than 25% for $\sqrt{\hat{s}} > 425\,\mathrm{GeV}$, which corresponds to $p_T > 195\,\mathrm{GeV}$. In this range, all other subleading terms still contribute more than 7%. For $\sqrt{\hat{s}} > 330\,\mathrm{GeV}$ (i.e. $p_T > 143\,\mathrm{GeV}$), the contribution of the tree-level squared amplitude alone falls below 50%.

In order to represent effects of b quarks as complete as possible, we always take them into account in quark loop graphs contributing to gluon fusion and all light quark parton processes using the pole mass m_b. Furthermore, we adopt the five-flavour scheme for the description of b quark parton process. Working in the five-flavour scheme, we consider a set of parton distribution functions (PDFs) which uses a perturbatively defined b-quark PDF where, in the procedure of fitting free parameters in the light-quark and gluon PDFs to

[2] For the bottom-gluon scattering cross section we study here, we see that the contribution from interference of the tree-level and top-loop QCD graphs is of order $\alpha_b \sqrt{\alpha_t}$ and thus further "Yukawa-suppressed" than all other terms we take into account. This is the formal justification for retaining bottom-mass dependence only in the Yukawa coupling and using $m_b = 0$ otherwise, which makes the interference contribution vanish.

experimental results, also b-sensitive observables have been considered. Virtually all modern PDF sets are five-flavour PDF sets. Using b-quark PDFs in the five-flavour scheme for predicting the $H + 1$ b-jet production cross section is well justified by the good agreement of the NLO QCD result in this scheme with the corresponding NLO QCD result calculated in a four-flavour scheme [16, 24]. In the latter approach, among the quark flavours only u, d, s, c are considered to be distributed in the proton while final state bottom quarks can only appear through gluon-initiated processes.

We consider the b-quark to be a massless parton to be consistent with the parton model but retain a non-zero Yukawa coupling y_b. Specifically for the b quark parton process, we use the running $\overline{MS}$ mass at NLO QCD for the bottom quark,

$$m_b^2(\mu_R) = m_b^2 \left\{ 1 - 2\,\frac{\alpha_S}{\pi} \left[\log\left(\frac{\mu_R^2}{m_b^2}\right) + \frac{4}{3} \right] \right\} ,$$

as the mass parameter in y_b and we choose the factorisation scale $\mu_F^{(b)} = m_h/4$. In this way, the prediction for the tree level bottom-gluon scattering cross section gives a good approximation to the NLO QCD result [16, 25, 26].

4 Numerical results for hadronic cross sections

Hadron colliders like the LHC (Tevatron) collide protons with protons (anti-protons) with a total energy $\sqrt{s}$ in the laboratory frame. Hadronic cross sections are obtained via convolution of the parton-level cross sections with the parton distribution functions (PDFs) and summation over the various contributing partons. Experimental restrictions to the detectability of the produced particles are conventionally realized by imposing specific cuts to the kinematically allowed phase space. Typically, cuts are imposed on the final-state transverse momentum and/or the pseudorapidity in order to have high-p_T jets not too close to the beam axis. In our case, we choose the selection criteria,

$$p_T > p_T^{\min} , \qquad\qquad |\eta_{\rm jet}| < \eta_{\max} , \tag{7}$$

where p_T and $\eta_{\rm jet}$ denote transverse momentum and pseudorapidity of the final state parton. We evaluate the differential hadronic cross sections $d\sigma_{AB}/dp_T$ and $d\sigma_{AB}/d\eta_{\rm jet}$ (with $AB = pp$ or $p\bar{p}$) in the presence of those cuts as described in detail in [21].

The numerical evaluation has been carried out with the NLO MSTW2008 PDFs [27] and a consistently chosen strong coupling constant $\alpha_S(\mu_R)$, i.e. using the formula including the NLO QCD corrections (see e.g. Ref. [28]) for $n_f = 5$ with $\alpha_S(m_Z) = 0.1201789$. The renormalisation scale μ_R and factorisation scale for the gluon and the light quarks μ_F are chosen both equal to m_h. For the bottom-quark factorisation scale $\mu_F^{(b)}$ we choose $m_h/4$. In the calculation, the pole masses for the top and bottom quark are set to the values

$$m_t = 171.3\,\text{GeV} , \qquad\qquad m_b = 4.2\,\text{GeV} ,$$

while the values of the electroweak parameters are chosen as

$$m_W = 80.398\,\text{GeV}\,, \qquad m_Z = 91.1876\,\text{GeV}\,, \qquad G_F = 1.16637 \cdot 10^{-5}\,\text{GeV}^{-2}\,,$$
$$\cos\theta_w = \frac{m_W}{m_Z}\,, \qquad \alpha = \frac{\sqrt{2}}{\pi} G_F m_W^2 \sin^2\theta_w\,.$$

The CKM matrix is assumed to be diagonal. We have evaluated the partonic cross sections with the help of the computer programs FeynArts 3.2 and FormCalc 3.2[3] [29] and further convoluted them with PDFs according to formulae given in [21]. For the evaluation of the NLO MSTW2008 PDFs [27] and the corresponding $\alpha_S(\mu_R)$ we used LHAPDF [30].

4.1 Tevatron

For the numerical evaluation of all cross sections we use $\sqrt{s} = 1.96\,\text{TeV}$ and the cuts in Eq. (7) with $p_T^{\text{min}} = 15\,\text{GeV}$ (as in Ref. [18]) and $\eta_{\text{max}} = 2.5$, i.e. we use the former (latter) in the calculation of η (p_T) distributions. At the Tevatron, the contributions of quark-gluon scattering and gluon fusion to the Higgs plus jet cross section are comparable in size, e.g. for $m_H = 120\,\text{GeV}$ and the given cuts, quark-gluon scattering contributes in total 41.5% and bottom-gluon scattering alone 1.4%. Furthermore, $q\bar{q}$ annihilation contributes in total 4.5% and $b\bar{b}$ annihilation alone 0.23%. We start by presenting the impact of electroweak loops and b-quark processes on the differential cross section predictions for quark-gluon scattering and quark–anti-quark annihilation separately.

4.1.1 Quark-Gluon Scattering

Fig. 5(a) shows the jet transverse momentum (p_T) distribution of Higgs plus jet production via quark-gluon scattering calculated in four approximations: either including or neglecting electroweak loop contributions combined with either including or neglecting the b-quark parton contributions in the prediction, represented by the identifiers "`all`", "`all, no b`", "`QCD`" and "`QCD, no b`" in the Figure. For comparison, the contributions of gluon fusion (including top- and bottom-loop graphs in the amplitude) and of bottom-gluon scattering to the Higgs plus jet cross section are also shown in Fig. 5(a). Among the parton contributions to the Higgs plus jet p_T distribution, quark–gluon scattering is the largest contribution for p_T above about 80 GeV, while gluon fusion dominates at lower p_T. The relative contribution of electroweak loops is very small at low p_T and increases with rising p_T, while it is the other way around with the contributions of b-quark parton processes.

Fig. 5(b) shows relative differences Δ between the four approximations to the quark-gluon scattering cross section displayed in Fig. 5(a). The effect of including electroweak contributions depends on p_T (dashed line) and the overall effect ranges from +5% to -12%

[3]The results are corrected for a documented bug (see file "ChangeLog" in FormCalc version 5.3 or newer for details) in the calculation of a particular type of colour factor appearing in the gluon-fusion amplitude.

for $10\,\text{GeV} < p_T < 200\,\text{GeV}$. The effect of the electroweak loops contributing to the b-quark processes amounts to a slight rise of the Higgs plus jet cross section by at most 2%. It is approximately given by the difference between the dashed and dotted lines in Fig. 5(b), where the latter represents the relative effect of electroweak loops in the light-quark parton processes only which corresponds to (and agrees with) results of Ref. [18].

Fig. 5(c) shows the bottom-gluon scattering cross section alone calculated in four approximations. While the identifier "`bg, all`" in Fig. 5(c) corresponds to retaining all contributions to the amplitude non-zero in Eq. (3), "`bg, QCD`" corresponds to setting E, C, F to zero, i.e. the amplitude is approximated by the tree-level graphs in Fig. 1(d) and the top-loop graphs in Fig. 1(b). The identifier "`bg, tree`" indicates that only the tree-level amplitude is considered, i.e. only D in Eq. (3) is non-zero, and "`bg, loops only`" corresponds to setting only D to zero. In the p_T range displayed, none of the contributions to bottom-gluon scattering is negligible.

For the prediction of the p_T distribution of bg scattering, it turns out that discarding the squared top-loop graphs in the cross section prediction ($\propto \alpha_t$ in Eq. (6)), because their contribution is formally of higher order in α_S, as has often been done in the past, is a bad approximation for larger p_T values. Although this contribution to the partonic bg cross section is smaller than the tree-level contribution at low centre-of-mass energy $\sqrt{\hat{s}}$, it has a flatter energy dependence. Thus, it becomes larger than the tree-level contribution beyond a certain energy $\sqrt{\hat{s}_0}$. For instance, for $m_H = 120\,\text{GeV}$ and a cut on the scattering angle $10^\circ < \hat{\theta} < 170^\circ$, we get $\sqrt{\hat{s}_0} = 430\,\text{GeV}$ and for $\sqrt{\hat{s}} > 260\,\text{GeV}$ the top-loop contribution is already more than 50% of the tree-level contribution (see Fig. 4). The situation is similar for the contribution of electroweak loop graphs. Taking those into account as well, the turnover point where the loop-squared becomes larger than the tree-squared is $\sqrt{\hat{s}_0} = 330\,\text{GeV}$ and for $\sqrt{\hat{s}} > 230\,\text{GeV}$ the loop contribution is $> 50\%$ of the tree-level contribution. As final state jets with a certain p_T introduce the energy threshold

$$\sqrt{\hat{s}} > p_T + \sqrt{m_H^2 + p_T^2} =: \sqrt{\hat{s}_{\text{low}}}\,, \tag{8}$$

the above behaviour implies that for $p_T > 198\,[143]\,\text{GeV}$ top-quark [electroweak and top-quark] loop contributions dominate the p_T distribution. Therefore, we argue that these loop contributions, which do not interfere with the tree-level cross section for $m_b = 0$, need to be taken into account for an accurate leading order prediction of the bottom–gluon scattering contribution to Higgs plus jet. While a mere QCD power counting would suggest otherwise, clearly, the hierarchy of Yukawa couplings in the SM also suggests not to discard loop-squared parts $\propto \alpha_t$ in the cross section prediction.

Fig. 6 shows the same breakdown of contributions as the previous Figure, now for the pseudorapidity distribution $d\sigma/d\eta$ of the final state jet. Electroweak and b-quark parton contributions depend strongly on η (dashed and solid line in Fig. 6(b)) and are roughly of the same order (but opposite sign) with extrema of about -4% and 9%, respectively, at $\eta = 0$, i.e. for a jet radiated into the central part of the detector. The explanation of the strong η dependence of these contributions has two elements. One element is the appearance of Feynman graph topologies in the amplitudes with different angular dependence than in

the dominant light-quark QCD amplitudes. The other is the different angular dependence in the laboratory frame caused by parton collisions which have preferentially boosted final states due to unbalanced valence quark contributions (double-peak in $d\sigma/d\eta$ for light-quark–gluon scattering) as compared to parton collisions with no valence quarks involved (central peak in $d\sigma/d\eta$ for bottom–gluon scattering).

The bg scattering contribution to the η distribution in Fig. 6(c) illustrates how much the large contribution of loop-squared terms (QCD top-loop and electroweak) to the p_T distribution in Fig. 5(c) contribute significantly to $d\sigma/d\eta$, i.e. after p_T integration for given η. The bottom-gluon scattering cross section prediction including electroweak and top-loop graphs in the amplitude (solid line) is about 40% larger than the tree-level prediction (dotted line) at $\eta = 0$. The bulk of the contributions comes from including the top-loop graphs (dot-dashed line) which leads to a prediction that deviates from the full result for bg scattering only by about -5%.

4.1.2 Quark–Anti-Quark Annihilation

Fig. 7(a) shows the jet p_T distribution via the $q\bar{q}$ annihilation channel calculated in the same four approximations as described in the previous Section (4.1.1). Also here, the hadronic cross section via gluon fusion and $b\bar{b}$ annihilation are shown for comparison. Bottom quarks dominate the $q\bar{q}$ contribution to Higgs+jet below $p_T \approx 35\,\text{GeV}$. The reason for this dominance is that $b\bar{b}$ annihilation is mediated at tree-level by t- and u-channel virtual b-quark exchange graphs (see Fig. 1(d)) which make the cross section large at small non-zero p_T and it would rise indefinitely for $p_T \to 0$. In contrast to that, the contributions from light-quark parton processes vanish in this limit. This rise of the $b\bar{b}$ annihilation cross section for small p_T is analogous to the situation for the gluon-fusion and quark-gluon scattering process, where t- or u-channel virtual gluon exchange graphs cause a similar behaviour. In the low p_T region, soft gluon resummation is called for in order to obtain a reliable prediction. However, we do not expect that the relative sizes of different contributions to the Higgs plus jet cross section, which is our main concern here, are altered greatly by resummation effects.

The contribution of $q\bar{q}$ annihilation reaches the size of gluon fusion above $p_T \approx 140\,\text{GeV}$. Remarkably, this contribution rises with p_T up to about 150 GeV despite the fact that the parton luminosity is falling at the same time. This behaviour is caused by a pronounced threshold peak in the energy dependence of the partonic cross sections for $q\bar{q} \to Hg$ ($q = u, d, s, c$) which enters the phase space integration over jet final states with a given p_T. The threshold peak is located around $\sqrt{\hat{s}} = 2m_t =: \sqrt{\hat{s}_{\text{peak}}}$ and is due to the top-loop graphs of the QCD part of the amplitude [4]. The influence of this peak on the hadronic p_T distributions is strong if it occurs near the energy threshold for jets with given p_T: $\sqrt{\hat{s}_{\text{low}}}$ in Eq. (8). Equating $\sqrt{\hat{s}_{\text{peak}}} = \sqrt{\hat{s}_{\text{low}}}$, we get the transverse momentum where the peak exactly occurs at the boundary of the integration over jet phase space:

$$p_T^{\text{peak}} = m_t \left(1 - \frac{m_H^2}{4m_t^2}\right) \approx 150\,\text{GeV}\,.$$

Approaching p_T^{peak} from below, the double effect of the PDFs falling with rising $\sqrt{\hat{s}_{\text{low}}}$ and the cross section for $\sqrt{\hat{s}} \gtrsim \sqrt{\hat{s}_{\text{low}}}$ rising because of the peak moving closer towards $\sqrt{\hat{s}_{\text{low}}}$ is an overall rise of the p_T distribution. For $p_T > p_T^{\text{peak}}$, the peak region falls outside of the region of jet phase space integration and thus $d\sigma/dp_T$ drops sharply.

Fig. 7(b) and 7(c) show relative differences between results of the four approximations. In particular, Fig. 7(b) zooms in on the special area $p_T < 40\,\text{GeV}$. Naturally, as the quark annihilation contribution of b-quarks rises and of light quarks vanishes with $p_T \to 0$, respectively, the relative contribution of the b-quark processes (solid line) reaches almost a factor of 100 at $p_T = 10\,\text{GeV}$. While the electroweak contributions to the light-quark processes lead to large and negative interference (dotted line) at low p_T (e.g. -37% for $p_T = 20\,\text{GeV}$), the electroweak contributions to the b-quark processes are much smaller in the same p_T region (e.g. $+2\%$ for $p_T = 20\,\text{GeV}$). Hence, with increasing dominance of the b-quark processes towards lower p_T, the relative contribution of electroweak loops in the sum of all quarks (dashed line) is diminished. We confirm the results for the electroweak loop effects in the light-quark $q\bar{q}$ annihilation processes [18] but also demonstrate the importance of including the b-quark initiated processes as well.

In Fig. 7(d), a breakdown of different contributions to the p_T distribution of the $b\bar{b}$ annihilation process analogous to the one in Fig. 5(c), described in Section 4.1.1, demonstrates the smallness of all loop contributions below $p_T \approx 120\,\text{GeV}$. From this information, one can already conclude that the η distribution for the given cut of $p_T > 15\,\text{GeV}$ will be practically independent of the loop contributions. The hadronic cross section via $b\bar{b}$ using only loop graphs in the amplitude (dashed line), shows qualitatively similar behaviour with p_T as the light-quark annihilation cross section. This is also due to a threshold peak caused by top-loop graphs in the partonic scattering amplitude, as explained above.

In Fig. 8, the η distribution of the $q\bar{q}$ annihilation channel is shown split in separate contributions as in previous figures. The hadronic cross section via $q\bar{q}$ calculated taking electroweak and b-quark contributions into account (solid line in Fig. 8(a)) and neglecting them both ($\times$-dashed line) are roughly equal. This shows that for the given kinematical cuts, electroweak and b-quark contributions roughly compensate each other, as can be seen more quantitatively in Fig. 8(b). Fig. 8(c) demonstrates the expected smallness of the loop contributions to the $b\bar{b}$ channel.

4.1.3 Corrections to Higgs + Jet Distributions

We discuss the impact of contributions from electroweak loops and b-quark parton processes on the total Higgs plus high-p_T jet cross section, i.e. the sum of the gluon fusion, quark-gluon scattering and $q\bar{q}$ annihilation contribution. Figs. 9(a) and 9(b) show the relative size of the contributions to the p_T and η distribution, respectively, for three different Higgs masses: $m_H = 120\,\text{GeV}$, $160\,\text{GeV}$ and $200\,\text{GeV}$. A feature, both present in the p_T and the η distribution, is that the b-quark contributions decrease and electroweak contributions increase with rising Higgs mass. In general, effects on the p_T distribution (see Fig. 9(a)) by b-quark contributions (black lines) decrease and electroweak contributions (green lines) increase with p_T. The largest effect of b-quark processes amounts to an increase of about

3% at low p_T for $m_H = 120\,\text{GeV}$. The largest effect of the electroweak contributions is a decrease of about -14% for p_T-values in the range 110 to 160 GeV and $m_H = 200\,\text{GeV}$.

Fig. 9(b) shows the impact of electroweak and b-quark contributions on the η distribution. Both contributions have their largest magnitude at $\eta = 0$: $+2.5\%$ for $m_H = 120\,\text{GeV}$ for the b-quark contribution and -5.3% for $m_H = 200\,\text{GeV}$ for the electroweak contribution.

4.2 LHC

For the numerical evaluation of all cross sections we use $\sqrt{s} = 10\,\text{TeV}$ and the cuts in Eq. (7) with $p_T^{\text{min}} = 30\,\text{GeV}$ and $\eta_{\text{max}} = 4.5$ which have been used in previous SM studies for the LHC [5, 6]. At the end of Section 4.2.3 we make some comments on the $\sqrt{s}$ dependence of the results. At the LHC, gluon fusion dominates largely over quark-gluon scattering and the $q\bar{q}$ annihilation contribution is quite small, e.g. for $m_H = 120\,\text{GeV}$ and the given cuts, quark-gluon scattering and $q\bar{q}$ annihilation contribute 27.8% and 0.8%, respectively, to the total Higgs plus jet cross section. The contribution of bgscattering and $b\bar{b}$ annihilation alone is 2% and 0.3%, respectively. Note that detailed descriptions of certain common features of the results which have been already given for the Tevatron case in Section 4.1 will not be given for the LHC case.

4.2.1 Quark-Gluon Scattering

Fig. 10(a) shows the p_T distribution of Higgs plus jet production via quark-gluon scattering calculated in the four approximations ("`all`", "`all, no b`", "`QCD`" and "`QCD, no b`") described in Section 4.1.1. The hadronic cross section via gluon fusion and bottom-gluon scattering are also shown in Fig. 10(a) for comparison.

Similar to the Tevatron case, the relative contribution of electroweak loops, shown in Fig. 10(b), is very small at low p_T and increases with rising p_T, while it is the other way around for the b-quark contributions. The electroweak contribution (dashed line) ranges from $+0.4\%$ to -6% in the displayed p_T interval from 10 GeV to 200 GeV. The relative b-quark contribution (solid line) ranges from 20% at low to 4.7% at high p_T.

The effect of the electroweak loops contributing to the b-quark processes, which cause an increase of about 40% of the cross section for these subprocesses for $p_T > 100\,\text{GeV}$ (see Fig. 10(c)), amounts to a slight rise of the total Higgs+jet cross section by at most 2.5% for p_T above 100 GeV.

Fig. 10(c) shows the bottom-gluon scattering cross section alone calculated in four approximations ("`bg, all`", "`bg, QCD`", "`bg, tree`", and "`bg, loops only`") described in Section 4.1.1. In the p_T range displayed, similar to the Tevatron case, none of the contributions is negligible, confirming results of Ref. [19].

Fig. 11 shows the same breakdown of contributions as the previous Figure, for the jet pseudorapidity distribution $d\sigma/d\eta$. Electroweak and b-quark parton contributions depend

strongly on η (dashed and solid line in Fig. 11(b)) and have extrema of about -4% and $+16.5\%$, respectively, at $\eta = 0$.

4.2.2 Quark–Anti-Quark Annihilation

Fig. 12(a) shows the jet p_T distribution via the $q\bar{q}$ annihilation channel calculated in the same four approximations as described in Section 4.1.1 and of the gluon fusion and $b\bar{b}$ annihilation channel for comparison. As the qualitative behaviour of this channel is similar to the Tevatron case, we refer to Section 4.1.2 for their explanation. The $b\bar{b}$ contribution dominates the $q\bar{q}$ contribution to the Higgs+jet cross section below $p_T \approx 65\,\text{GeV}$. This dominance is even more pronounced than in the Tevatron prediction (see Section 4.1.2) and is again due to tree-level t- and u-channel virtual b-quark exchange graphs (see Fig. 1(d)). This contribution would rise indefinitely for $p_T \to 0$ while the contribution from light-quark parton processes vanish in this limit.

Fig. 12(b) and 12(c) show relative differences between results of the four approximations. In particular, Fig. 12(b) zooms in on the special area $p_T < 80\,\text{GeV}$. Naturally, as the annihilation contribution of b-quarks rises and of light quarks vanishes with $p_T \to 0$, respectively, the relative contribution of the b-quark processes (solid line) reaches a factor of about 370 at $p_T = 10\,\text{GeV}$. However, the b-quark contribution is not only relevant in the low p_T region, in which soft gluon resummation is called for in order to obtain a reliable prediction. It stays above 20% up to $p_T \approx 95\,\text{GeV}$ which is where it first falls behind the electroweak contributions in significance.

While the electroweak contributions to the light-quark processes lead to large and negative interference (dotted line) at low p_T (e.g. -34% for $p_T = 20\,\text{GeV}$), confirming results of [18], the electroweak contributions to the b-quark processes alone, in the same p_T region, are very small (e.g. $+1\%$ for $p_T = 20\,\text{GeV}$). Hence, the increasing dominance of the b-quark processes towards lower p_T leads to a decrease of the relative contribution of electroweak loops in the sum of all quark parton contributions (dashed line).

In Fig. 12(d), a breakdown of different contributions to the p_T distribution of the $b\bar{b}$ annihilation process analogous to Fig. 10(c) demonstrates that sizeable loop contributions to this process only set in above $p_T \approx 120\,\text{GeV}$.

In Fig. 13, the η distribution of the $q\bar{q}$ annihilation channel is shown split in separate contributions as in previous Figures. The fact that electroweak and b-quark contributions are sizeable is reflected by the clear separation of all lines in Fig. 13(a). For the given cut of $p_T > 30\,\text{GeV}$, the b-quark contribution (solid line in Fig. 13(b)) still reaches 77% at $\eta = 0$, while the electroweak contribution (dashed line) varies between -20% and -11% with a minimum at $\eta = 0$. Similar to the Tevatron case, loop contributions do not affect the η distribution of the $b\bar{b}$ channel for the given cuts (see Fig. 13(c)).

4.2.3 Corrections to Higgs + Jet Distributions

Having studied the effects of electroweak loops and b-quark processes on quark-gluon scattering and $q\bar{q}$ annihilation separately, we discuss here the impact of those contributions

on the total Higgs plus high-p_T jet cross section. Figs. 14(a) and 14(b) show the relative size of the contributions to the p_T and η distribution, respectively, for three different Higgs masses: $m_H = 120\,\text{GeV}$, $160\,\text{GeV}$ and $200\,\text{GeV}$. The qualitative features of the b-quark and electroweak contributions to the p_T and η distributions are similar to the Tevatron case, e.g. b-quark decrease and electroweak contributions increase with rising Higgs mass, respectively. On the quantitative level, the maximal effect of the electroweak loops on the p_T distribution (green lines in Fig. 14(a)) is diminished to a -3% change of the cross section in the range $p_T > 120\,\text{GeV}$ and for $m_H = 200\,\text{GeV}$, compared to -14% for the Tevatron case. The reason for this difference is that the qg and $q\bar{q}$ channels, which are affected at leading order by electroweak loops, dominate the Higgs + Jet cross section for large p_T at the Tevatron, while at the LHC (with $\sqrt{s} = 10\,\text{TeV}$) gluon fusion dominates over the full p_T range. Contrary to that, the b-quark contributions to the p_T distribution (black lines) are slightly higher throughout the displayed p_T range, reaching maximally $+3.5\%$ at low p_T for $m_H = 120\,\text{GeV}$.

Fig. 14(b) shows the impact of electroweak and b-quark contributions on the η distribution. Both contributions have their largest magnitude at $\eta = 0$: $+2.9\%$ for $m_H = 120\,\text{GeV}$ for the b-quark contribution and -2.0% for $m_H = 200\,\text{GeV}$ for the electroweak contribution. The large difference between the electroweak contributions for larger p_T values in the Tevatron and LHC case is not seen in the η distributions. This is to be expected, as the p_T range where the difference in $d\sigma/dp_T$ is substantial contributes only little to the cross section $d\sigma/d\eta$.

As the collision energy of the LHC will probably be changed a few times before the design goal of 14 TeV is reached, we have also studied the $\sqrt{s}$ dependence of the electroweak and b-quark contributions to the total Higgs plus jet cross section (with the given cuts: $p_T^{\text{min}} = 30\,\text{GeV}$ and $\eta_{\text{max}} = 4.5$) for the three Higgs masses 120 GeV, 160 GeV and 200 GeV. We find that the relative contributions depend only mildly on the collider energy. For instance, for $\sqrt{s}$ from 7 TeV to 14 TeV, the electroweak contributions for $m_H = 200\,\text{GeV}$ vary from -2.2% to -1.5% and the b-quark contributions for $m_H = 120\,\text{GeV}$ vary from $+2.3\%$ to $+2.45\%$. As is clear from Figs. 14(a) and 14(b), a tighter p_T-cut will increase the relative electroweak contribution while the relative b quark contribution will stay almost the same. A tighter η-cut will increase the relative size of both contributions.

5 Conclusions

We have calculated specific contributions to jet pseudorapidity and transverse momentum distributions for the Standard Model Higgs plus high-p_T jet production cross section at the LHC and the Tevatron. The remaining scale uncertainty of the NLO QCD prediction (in the large top-mass limit) for this Higgs production mode via light quark parton processes is at the level of 10% [12, 13]. Motivated by this, we discussed here the contributions of electroweak loops and of bottom-quark parton processes (in the five-flavour scheme)

to cross section predictions for the Tevatron and the Large Hadron Collider with 10 TeV collision energy.

For Higgs bosons with a mass of 120 GeV, 160 GeV and 200 GeV, we find the maximal effects of the electroweak contributions to the total Higgs plus jet p_T and η distribution to be -14% and -5.3%, respectively, for the Tevatron, and -3% and -2%, respectively, for the LHC. For the maximal contribution of bottom-quark parton processes to the p_T and η distribution, we find $+3\%$ and $+2.5\%$, respectively, for the Tevatron, and $+3.5\%$ and $+3\%$, respectively, for the LHC. Those contributions are smaller but still comparable in size to the numerical impact of including bottom quarks of non-zero mass in quark-loop mediated contributions to the Higgs plus jet cross section prediction. For both colliders, the magnitude of the electroweak contribution rises with Higgs mass, while the bottom parton contribution falls with Higgs mass.

A separate study of the Higgs + b-jet cross section demonstrates that a calculational approach which respects the hierarchies of Yukawa couplings yields a leading order cross section prediction which is more accurate in the high-p_T regime than conventional approaches.

A computer code corresponding to the calculation presented here will be made available with the next version release of the public code HJET [31].

Acknowledgements

I thank Frank Petriello for the efficient comparison of our numerical results. I thank Stefan Dittmaier, Alberto Guffanti, Karl Jakobs and Christian Schwinn for valuable comments and useful discussions. This work was supported by the Helmholtz Alliance HA-101 'Physics at the Terascale' and in part by the European Community's Marie-Curie Research Training Network under contract MRTN-CT-2006-035505 'Tools and Precision Calculations for Physics Discoveries at Colliders' (HEPTOOLS).

References

[1] G. Arnison *et al.* [UA1 Collaboration], Phys. Lett. B **122** (1983) 103; M. Banner *et al.* [UA2 Collaboration], Phys. Lett. B **122** (1983) 476; G. Arnison *et al.* [UA1 Collaboration], Phys. Lett. B **126** (1983) 398; P. Bagnaia *et al.* [UA2 Collaboration], Phys. Lett. B **129** (1983) 130.

[2] P. W. Higgs, Phys. Lett. **12** (1964) 132; Phys. Rev. Lett. **13** (1964) 508; Phys. Rev. **145** (1966) 1156; F. Englert and R. Brout, Phys. Rev. Lett. **13** (1964) 321; G. S. Guralnik, C. R. Hagen and T. W. B. Kibble, Phys. Rev. Lett. **13** (1964) 585.

[3] R. K. Ellis, I. Hinchliffe, M. Soldate and J. J. van der Bij, Nucl. Phys. B **297** (1988) 221; M. Chaichian, I. Liede, J. Lindfors and D. P. Roy, Phys. Lett. B **198** (1987) 416 [Erratum-ibid. B **205** (1987) 595].

[4] U. Baur and E. W. Glover, Nucl. Phys. B **339** (1990) 38.

[5] S. Abdullin, M. Dubinin, V. Ilyin, D. Kovalenko, V. Savrin and N. Stepanov, Phys. Lett. B **431** (1998) 410.

[6] V. V. Zmushko, ATL-PHYS-2002-020, IHEP-2002-23.

[7] B. Mellado, W. Quayle and S. L. Wu, Phys. Lett. B **611** (2005) 60.

[8] G. Aad *et al.* [The ATLAS Collaboration], CERN Report CERN-OPEN-2008-020, arXiv:0901.0512 [hep-ex].

[9] G. L. Bayatian *et al.* [CMS Collaboration], J. Phys. G **34** (2007) 995.

[10] C. Anastasiou, K. Melnikov and F. Petriello, Phys. Rev. Lett. **93** (2004) 262002, Nucl. Phys. B **724** (2005) 197.

[11] G. Bozzi, S. Catani, D. de Florian and M. Grazzini, Phys. Lett. B **564** (2003) 65; S. Catani, D. de Florian, M. Grazzini and P. Nason, JHEP **0307** (2003) 028.

[12] D. de Florian, M. Grazzini and Z. Kunszt, Phys. Rev. Lett. **82** (1999) 5209; V. Ravindran, J. Smith and W. L. Van Neerven, Nucl. Phys. B **634** (2002) 247; C. J. Glosser and C. R. Schmidt, JHEP **0212** (2002) 016.

[13] D. de Florian, A. Kulesza and W. Vogelsang, JHEP **0602** (2006) 047.

[14] J. Smith and W. L. van Neerven, Nucl. Phys. B **720** (2005) 182 [arXiv:hep-ph/0501098].

[15] J. Campbell, R. K. Ellis, F. Maltoni and S. Willenbrock, Phys. Rev. D **67** (2003) 095002; S. Dittmaier, M. Krämer and M. Spira, Phys. Rev. D **70** (2004) 074010.

[16] S. Dawson, C. B. Jackson, L. Reina and D. Wackeroth, Phys. Rev. Lett. **94** (2005) 031802 and Mod. Phys. Lett. A **21** (2006) 89.

[17] S. Dawson and P. Jaiswal, arXiv:1002.2672 [hep-ph].

[18] W. Y. Keung and F. J. Petriello, Phys. Rev. D **80** (2009) 013007.

[19] S. Mrenna and C. P. Yuan, Phys. Rev. D **53** (1996) 3547.

[20] O. Brein and W. Hollik, Phys. Rev. D **68** (2003) 095006.

[21] O. Brein and W. Hollik, Phys. Rev. D **76** (2007) 035002.

[22] B. Field, S. Dawson and J. Smith, Phys. Rev. D **69** (2004) 074013; B. Field, L. Reina and C. B. Jackson, Phys. Rev. D **76** (2007) 074008.

[23] U. Langenegger, M. Spira, A. Starodumov and P. Trueb, JHEP **0606** (2006) 035.

[24] J. M. Campbell *et al.*, arXiv:hep-ph/0405302; K. A. Assamagan *et al.* [Higgs Working Group Collaboration], arXiv:hep-ph/0406152; C. Buttar *et al.* [Standard Model and Higgs Working Group], arXiv:hep-ph/0604120.

[25] D. Dicus, T. Stelzer, Z. Sullivan and S. Willenbrock, Phys. Rev. D **59** (1999) 094016.

[26] D. Rainwater, M. Spira and D. Zeppenfeld, hep-ph/0203187; T. Plehn, Phys. Rev. D **67** (2003) 014018; F. Maltoni, Z. Sullivan and S. Willenbrock, Phys. Rev. D **67** (2003) 093005; E. Boos and T. Plehn, Phys. Rev. D **69** (2004) 094005; R. V. Harlander and W. B. Kilgore, Phys. Rev. D **68** (2003) 013001.

[27] A. D. Martin, W. J. Stirling, R. S. Thorne and G. Watt, arXiv:0901.0002 [hep-ph].

[28] W. M. Yao *et al.* [Particle Data Group], J. Phys. G **33** (2006) 1.

[29] J. Küblbeck, M. Böhm, A. Denner, Comput. Phys. Commun. **60** (1990) 165; H. Eck, Ph.D. thesis, University of Würzburg (1995); T. Hahn and M. Perez-Victoria, Comput. Phys. Commun. **118** (1999) 153; T. Hahn, Comput. Phys. Commun. **140** (2001) 418.

[30] M. R. Whalley, D. Bourilkov and R. C. Group, arXiv:hep-ph/0508110; `http://hepforge.cedar.ac.uk/lhapdf/`

[31] For updates, please consult the URL: `http://pheno.physik.uni-freiburg.de/~obr/`

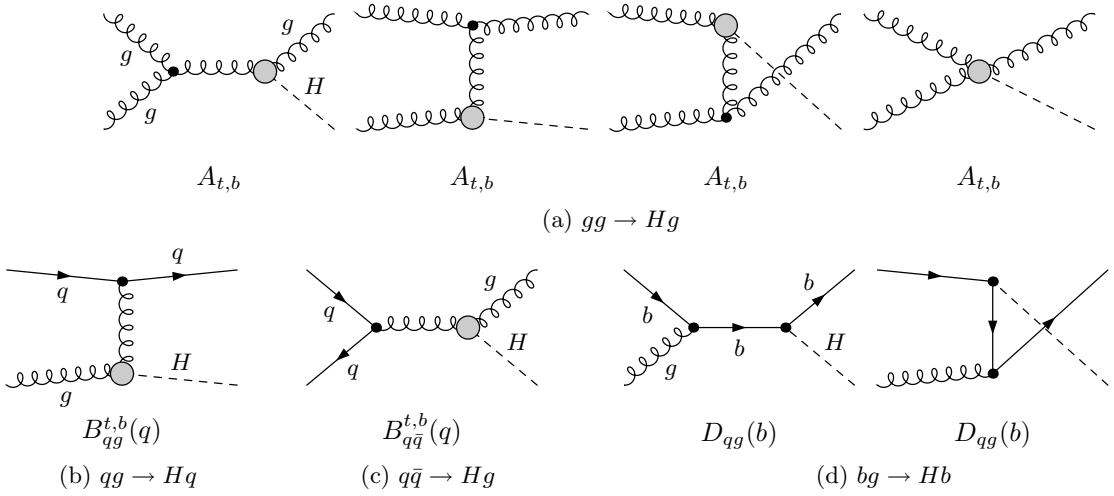

Figure 1: QCD contributions to the scattering amplitudes of the partonic subprocesses (a) $gg \to Hg$, (b) $qg \to Hq$, (c) $q\bar{q} \to Hg$ ($q = u, d, s, c$) and (d) $bg \to Hb$ at leading order. The shaded blob represents a quark loop (only top- and bottom loops contribute significantly). The symbol below each graph indicates to which coefficient in the mathematical expressions for the amplitudes (Eqs. (1) and (2)) this graph contributes.

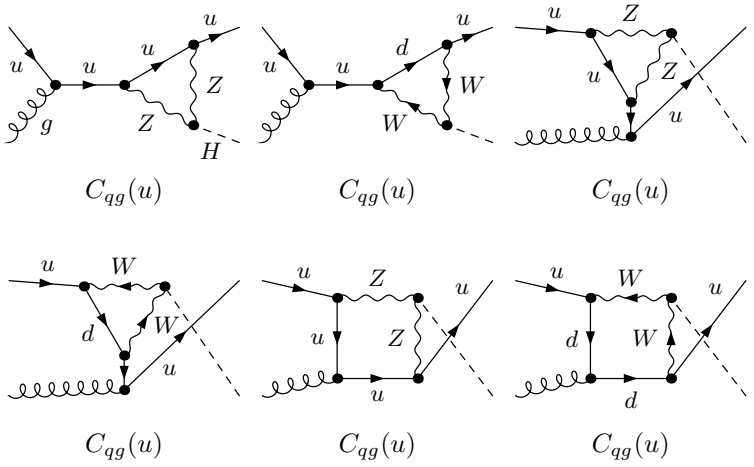

Figure 2: Electroweak loop contributions to the $ug \to Hu$ scattering amplitude at leading order, assuming no up-quark Higgs Yukawa coupling. The depicted graphs contribute all to the coefficient $C_{qg}(u)$ in the mathematical expression for the amplitude (Eq. (2)). The contributions look similar for the scattering of other quark flavours.

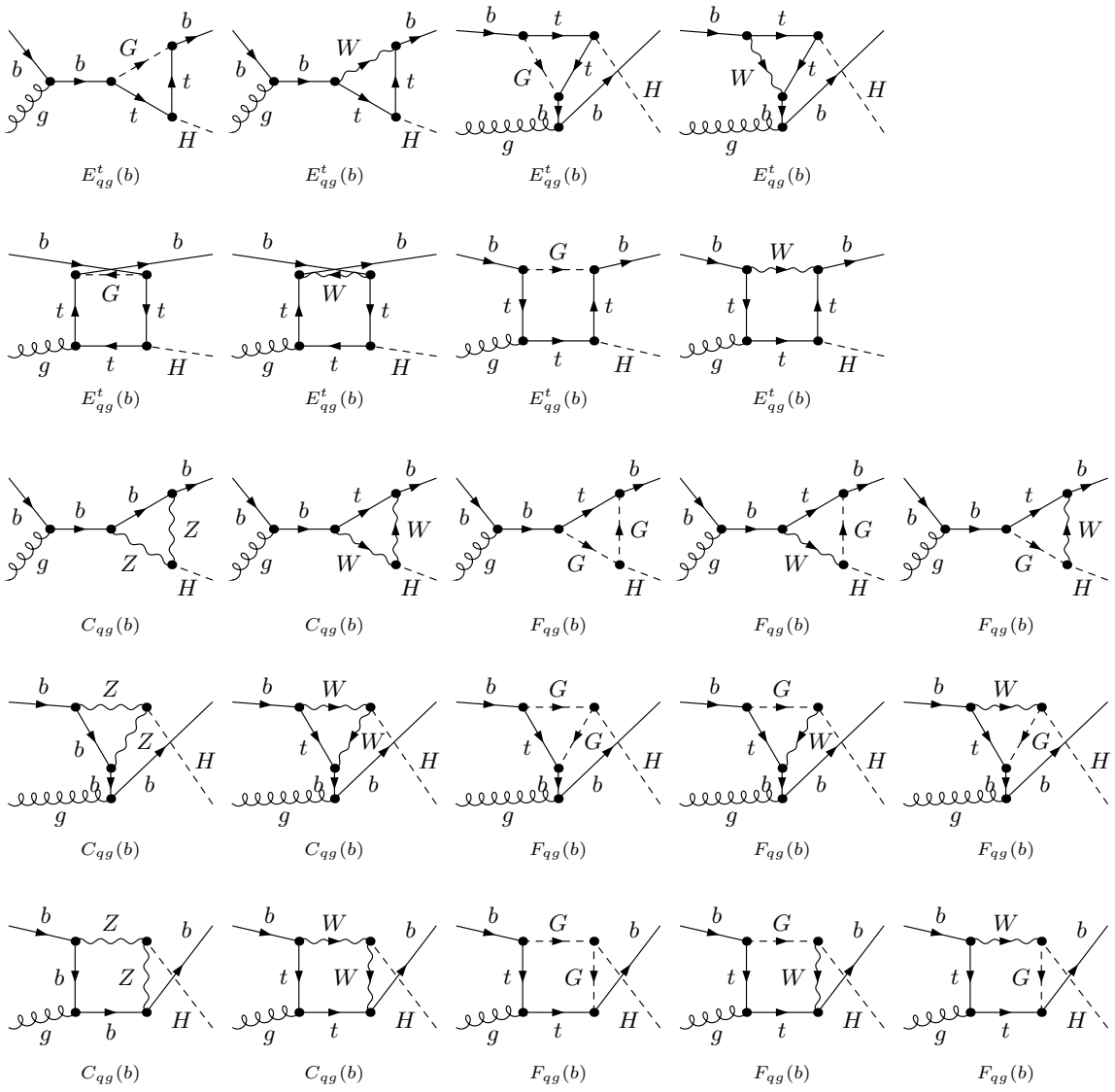

Figure 3: Electroweak loop contributions to the $bg \to Hb$ scattering amplitude at leading order which do not vanish for $m_b = 0$. The symbol below each graph indicates to which coefficient in the mathematical expression for the amplitude (Eq. (3)) this graph contributes.

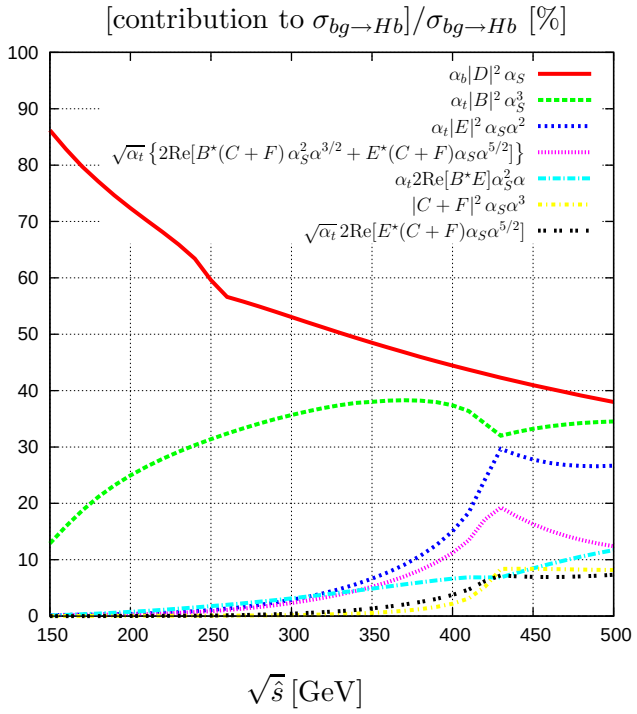

Figure 4: Relative contributions of different parts of the squared matrix element $|\mathcal{M}_{qg}(b)|^2$ (see Eq. (6)) to the integrated partonic cross section of $bg \to Hb$ as a function of centre-of-mass energy $\sqrt{\hat{s}}$ for $m_H = 120\,\mathrm{GeV}$ and a cut on the scattering angle $10^\circ < \hat{\theta} < 170^\circ$.

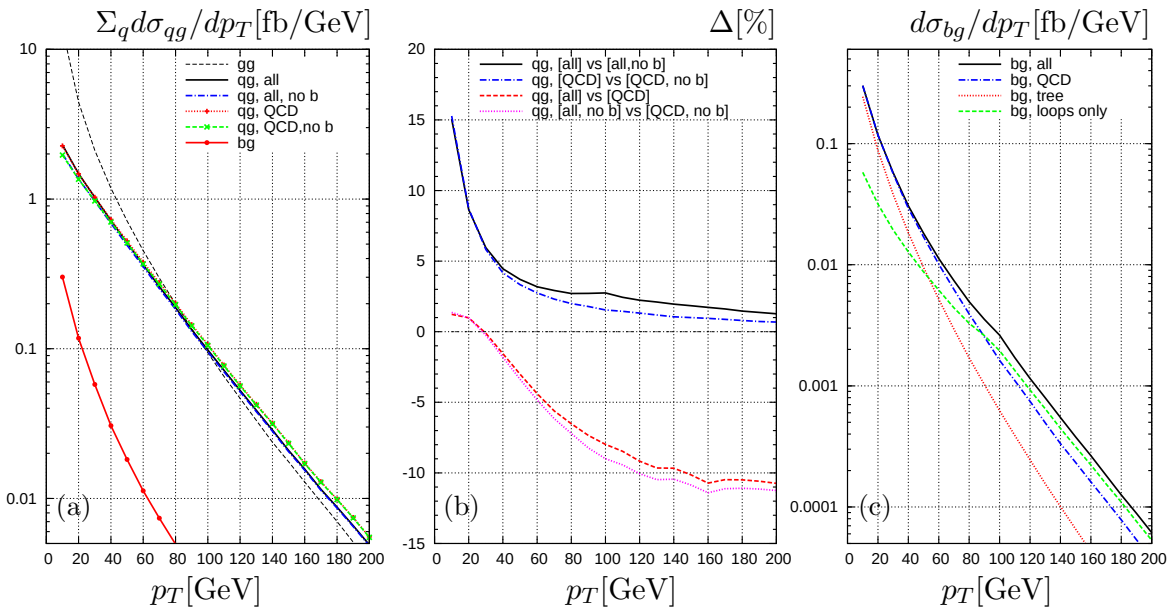

Figure 5: p_T distribution for quark-gluon scattering at the Tevatron: (a) quark parton processes with and without the b quark contributions, with and without electroweak contributions; (b) relative differences to the left panel; (c) contributions to the b quark parton processes. The depicted approximations are described in the main text.

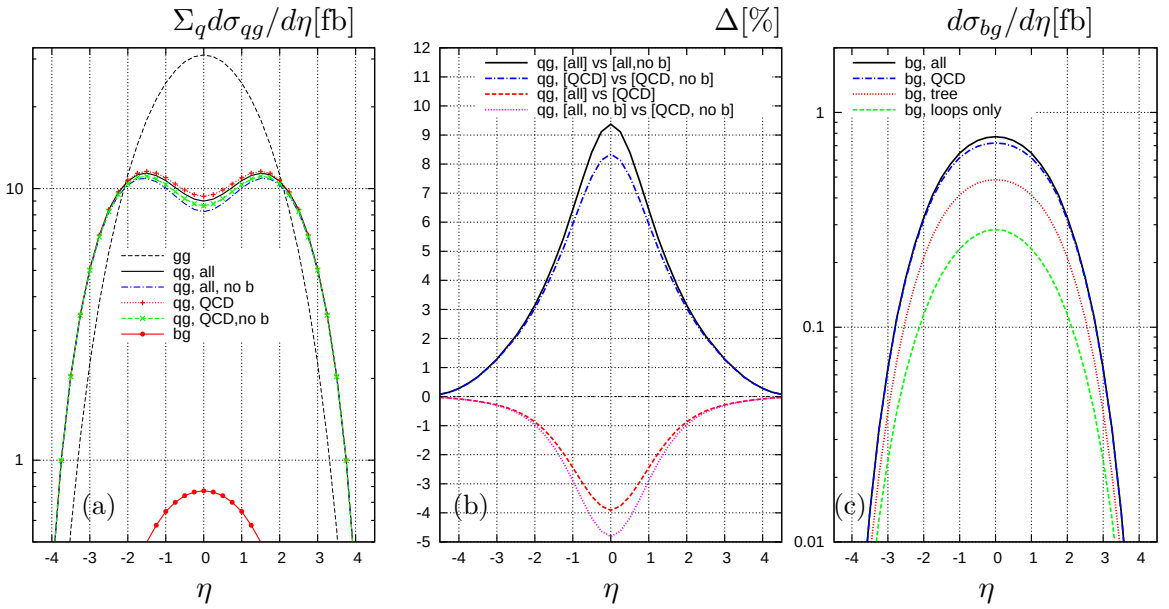

Figure 6: η distribution for quark-gluon scattering at the Tevatron: (a) quark parton processes with and without the b quark contributions, with and without electroweak contributions; (b) relative differences to the left panel; (c) contributions to the b quark parton processes. The depicted approximations are described in the main text.

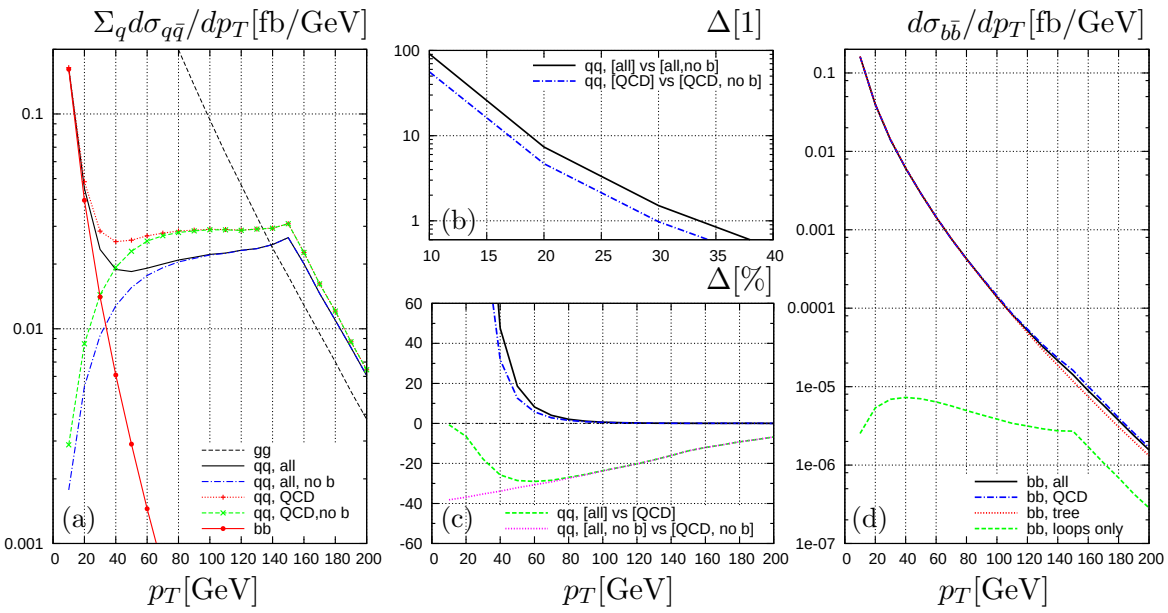

Figure 7: p_T distribution for quark–anti-quark annihilation at the Tevatron: (a) quark parton processes with and without the b quark contributions, with and without electroweak contributions; (b),(c) relative differences to the left panel; (d) contributions to the b quark parton processes. The depicted approximations are described in the main text.

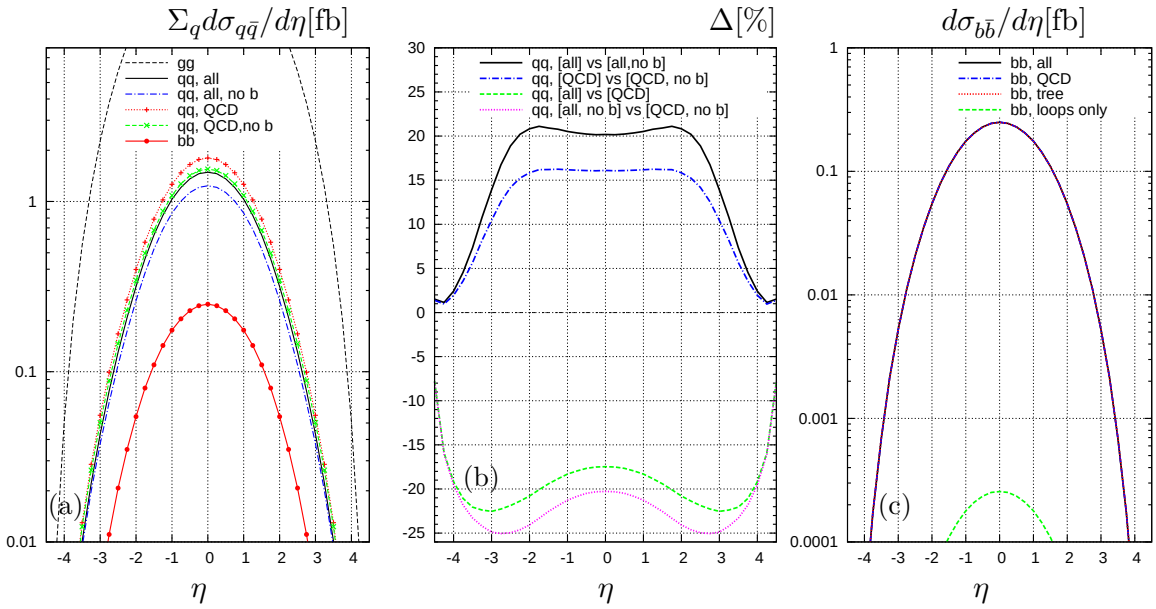

Figure 8: η distribution for quark–anti-quark annihilation at the Tevatron: (a) quark parton processes with and without the b quark contributions, with and without electroweak contributions; (b) relative differences to the left panel; (c) contributions to the b quark parton processes. The depicted approximations are described in the main text.

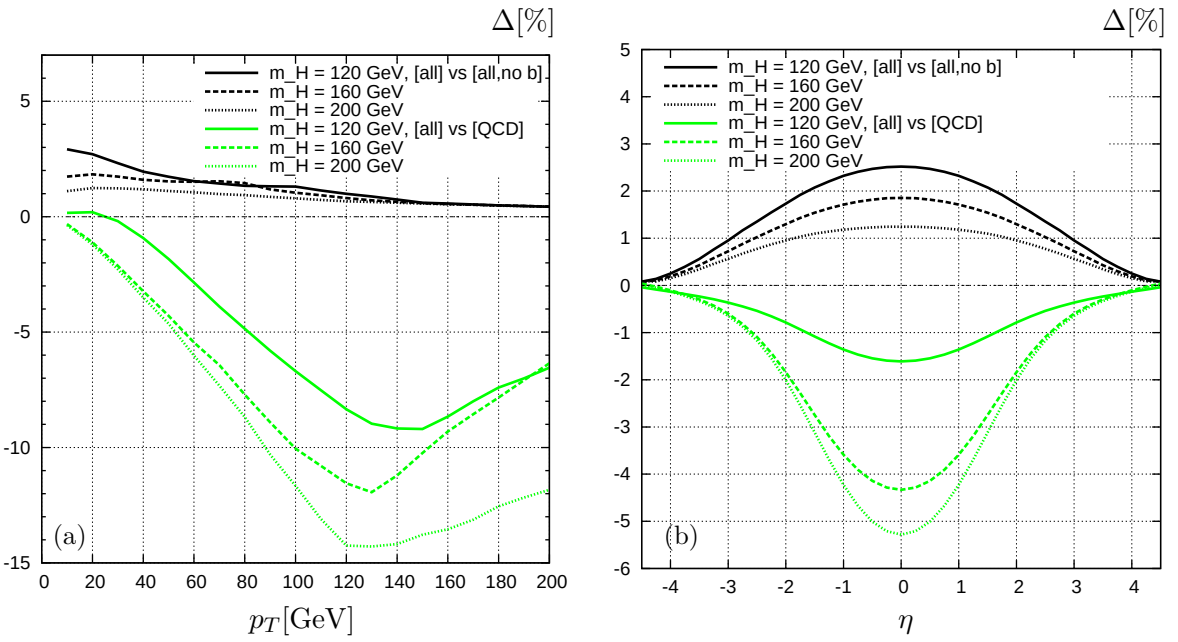

Figure 9: Relative size of the effects of including b-quark parton processes (black lines) and electroweak contributions (green lines) on the Tevatron ($\sqrt{s} = 1.96\,\text{TeV}$) differential distributions for Higgs + Jet production: (a) p_T distribution and (b) η distribution of the recoiling jet.

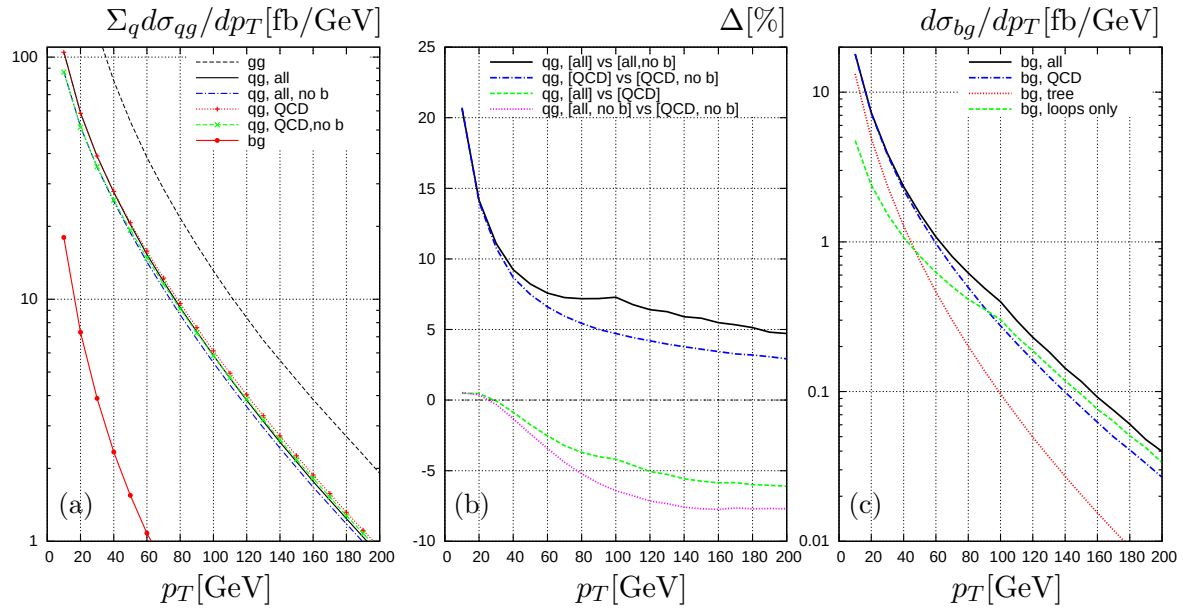

Figure 10: p_T distribution for quark-gluon scattering at the LHC ($\sqrt{s} = 10\,\text{TeV}$): (a) quark parton processes with and without the b quark contributions, with and without electroweak contributions; (b) relative differences to the left panel; (c) contributions to the b quark parton processes. The depicted approximations are described in the main text.

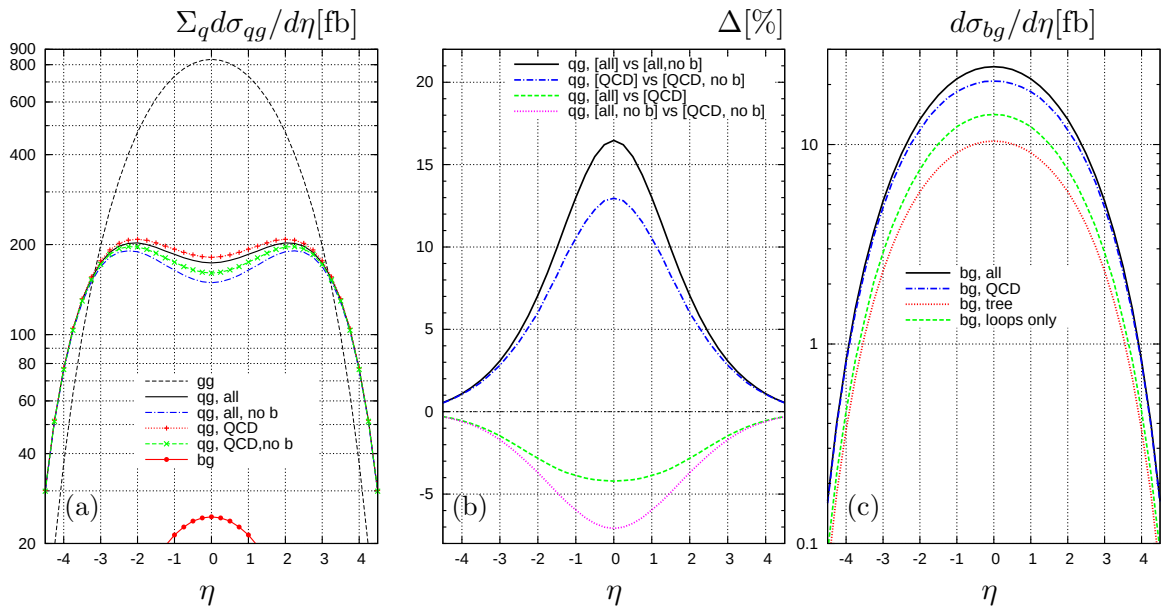

Figure 11: η distribution for quark-gluon scattering at the LHC ($\sqrt{s} = 10\,\text{TeV}$): (a) quark parton processes with and without the b quark contributions, with and without electroweak contributions; (b) relative differences to the left panel; (c) contributions to the b quark parton processes. The depicted approximations are described in the main text.

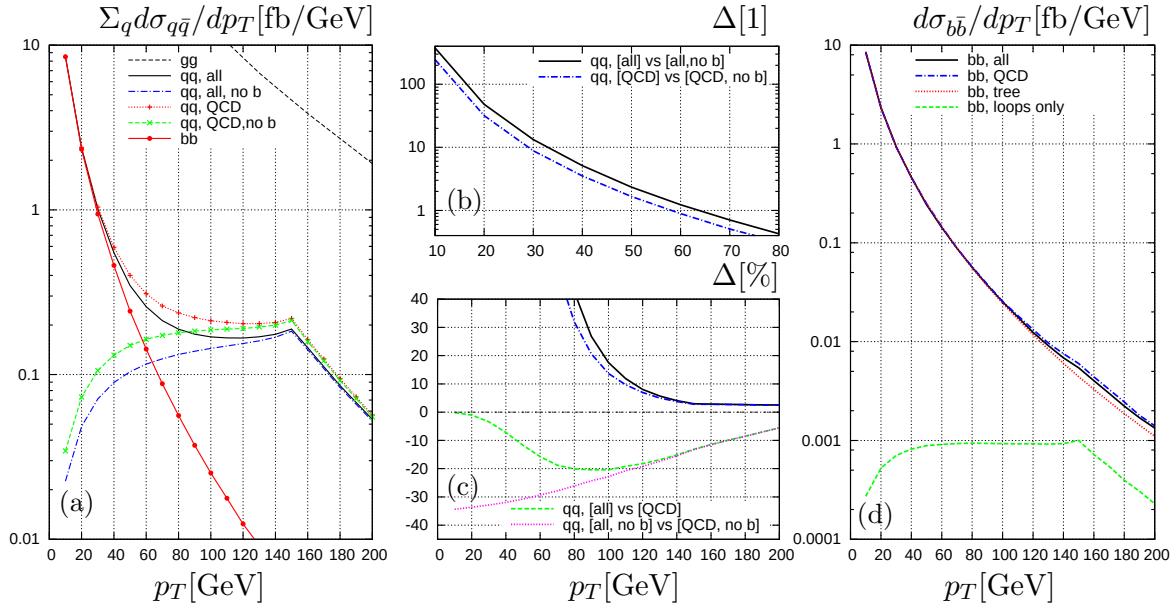

Figure 12: p_T distribution for quark–anti-quark annihilation at the LHC ($\sqrt{s} = 10\,\text{TeV}$): (a) quark parton processes with and without the b quark contributions, with and without electroweak contributions; (b) relative differences to the left panel; (c) contributions to the b quark parton processes. The depicted approximations are described in the main text.

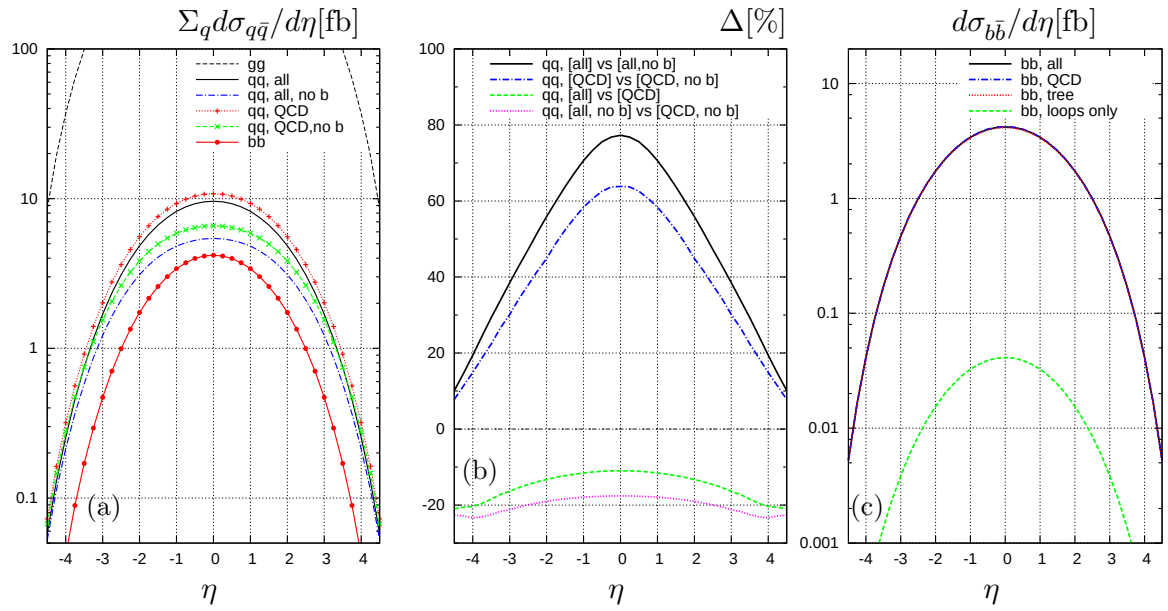

Figure 13: η distribution for quark–anti-quark annihilation at the LHC ($\sqrt{s} = 10\,\text{TeV}$): (a) quark parton processes with and without the b quark contributions, with and without electroweak contributions; (b) relative differences to the left panel; (c) contributions to the b quark parton processes. The depicted approximations are described in the main text.

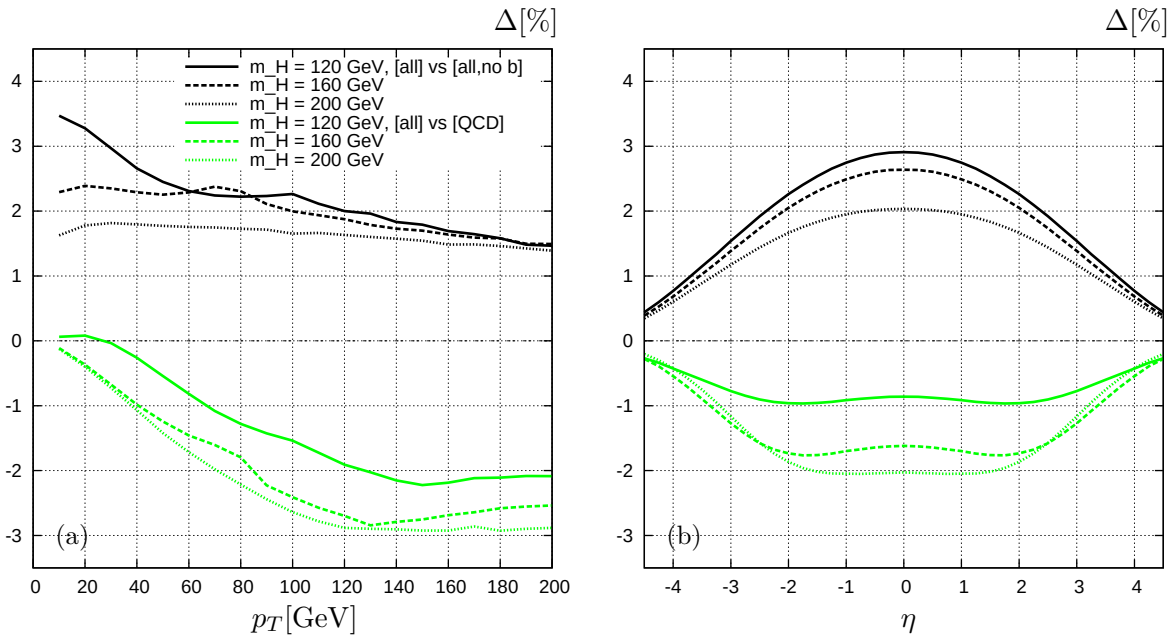

Figure 14: Relative size of the effects of including b-quark parton processes (black lines) and electroweak contributions (green lines) on the LHC ($\sqrt{s} = 10\,\text{TeV}$) differential distributions for Higgs + Jet production: (a) p_T distribution and (b) η distribution of the recoiling jet.